Chapter 12

Characterization of RNA Nanoparticles and Their Dynamic Properties Using Atomic Force Microscopy

Alexander J. Lushnikov, Yelixza I. Avila, Kirill A. Afonin, and Alexey V. Krasnoslobodtsev

Abstract

The protocol described in this chapter allows for acquiring topography images of RNA-based nanoring structures and assessing their dynamic properties using atomic force microscopy (AFM) imaging. AFM is an indispensable tool for characterization of nucleic acid-based nanostructures with the exceptional capability of observing complexes in the range of a few nanometers. This method can visualize structural characteristics and evaluate differences between individual structurally different RNA nanorings. Due to the highly resolved AFM topography images, we introduce an approach that allows to distinguish the differences in the dynamic behavior of RNA nanoparticles not amenable to other experimental techniques. This protocol describes in detail the preparation procedures of RNA nanostructures, AFM imaging, and data analysis.

Key words Atomic force microscopy, Topography imaging, RNA nanoparticle, Mica surface modification, Flexibility analysis, Mechanical stability

1 Introduction

Nucleic acid nanotechnology is a research area that uses nucleic acid assembly principles as the bottom-up nanotechnological approach. This includes DNA and RNA, with the examples of nano-assemblies (e.g., RNA fibers, RNA and DNA cubes, and RNA rings) [1–7] and macro-assemblies (e.g., DNA origami [8]) that use specifically designed sequences to controllably build functional structures [9, 10]. The ability to visualize and characterize small nanostructures is critical in gaining control over the complex assembly process and constructing nanostructures of predicted design. Small variations in size and composition of structural elements can lead to large variations in properties of nanomaterials. One of the methods capable of nanoscale characterization of small nanostructures is atomic force microscopy (AFM). This chapter demonstrates the ability of AFM to assess subnanometer variations

Kirill A. Afonin (ed.), *RNA Nanostructures: Design, Characterization, and Applications*, Methods in Molecular Biology, vol. 2709, https://doi.org/10.1007/978-1-0716-3417-2_12,

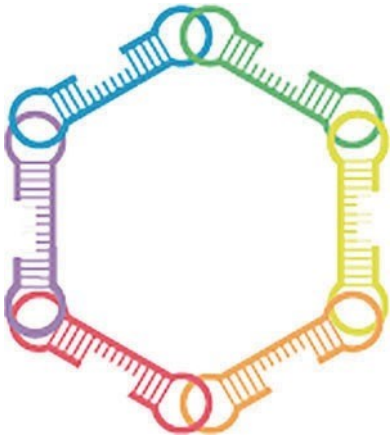

Fig. 1 Hexameric RNA nanostructure

in shapes of different nanostructures. Furthermore, we introduce a new approach to analysis of flexibility and dynamics of RNA-based hexameric nanorings modified with single strand gaps for potential functionalization of nanostructures.

Using the six computationally programmed dumbbell building blocks, the hexameric RNA nanostructures self-assemble into two-dimensional nanostructures. Stabilized by the colE1-like kissing loop interactions [11, 12], the nanostructures are designed to form highly symmetric nanoring structures (Fig. 1) [13]. The potential for further functionalization of such nanorings with little impact on the nanostructure's topology is increased by introducing gaps into the double-stranded regions of the RNA dumbbell monomers (Fig. 1). These gaps are only 6 bases long and, although small, can dramatically alter flexibility and dynamics of the entire nanoring structure.

Herein, we describe a method to evaluate the flexibility of the RNA nanorings via static AFM imaging and deformation analysis. With high-resolution AFM topography images, we can trace structural arrangement of individual monomeric dumbbells in highly resolved nanostructures [13]. All nanoring structures assume a flat orientation on the atomically smooth mica surface, allowing for a comparative analysis of their shapes. Most stable nanostructures appear nearly circular due to their symmetric design. Less stable structures tend to adopt more of an elliptical shape. Nanoring deformation can then be analyzed via cross-sectional analysis of the structures from high-resolution AFM images. The ratio of orthogonal elliptical axes (major, D_L, and minor, D_{SH}) drawn through the center of a nanoring reports on the degree of deformation, the nanoring experienced due to flexibility of monomeric dumbbells. We describe technical aspects of sample preparation and AFM imaging technique. The protocol is intended to help a user with basic level of AFM skills to obtain good quality images. Post-

acquisition image processing yields accurate information about distortion and deformation of the nanostructures reporting thus on their dynamic properties.

2 Materials and Equipment

Water quality and reagent purity are critically important for RNA nanoparticle preparation and high-resolution AFM imaging. Prepare all buffer solutions using ultrapure water (Milli-Q, ~18 MΩ-cm) and analytical grade reagents.

2.1 RNA Nanoparticle Preparation

1. DNA oligo sequences as desalted products were used without further purification.
2. MyTaq™ Mix for PCR amplification of DNA oligos.
3. The DNA Clean and Concentrator™ kit for PCR product purification.
4. Agarose and ethidium bromide for verification of purified DNA solutions.
5. Bio-Rad ChemiDoc MP System and ethidium bromide for band visualization in gels for analysis.
6. T7 RNA Polymerase.
7. "Transcription" buffer: HEPES-KOH, pH 7.5; 2.5 mM spermidine; 50 mM DTT; 25 mM $MgCl_2$; 5 mM rNTPs.
8. Acrylamide, bis-acrylamide, and TEMED for PAGE electrophoresis.
9. UV lamp for RNA band visualization.
10. Scalpel and tweezers for excision of gel pieces.
11. "Crush and soak" buffer: 300 mM NaCl, 89 mM Tris-borate (pH 8.2), 2 mM EDTA.
12. Nanodrop or spectrophotometer.
13. "Assembly" buffer: 89 mM tris-borate (pH 8.2), 2 mM $MgCl_2$, 50 mM KCl.
14. Heat blocks that can be held at constant temperatures of 95 °C and 30 °C.

2.2 Mica Preparation and Sample Deposition

1. Sharp scissors for cutting mica sheets.
2. Vacuum cabinet such as vacuum oven for storing AFM samples deposited on APS-modified mica under vacuum or argon atmosphere.
3. Ultra-high purity (99.999%) compressed argon.
4. Scotch™ tape for preparation of smooth mica substrates.
5. Double-sided adhesive tape for mounting samples on metal pucks.

6. 10 mm metal pucks for mounting mica substrates onto an AFM scanning stage.
7. Disposable plastic cuvettes for mica modification with APS and sample storage.

2.3 AFM Imaging and Data Analysis

1. MultiMode AFM Nanoscope IV system.
2. AFM probes RTESPA-300.
3. Data analysis FemtoScan Online Suite. *See* Note 1.
4. Software for statistical data analysis: MagicPlot Pro 3. *See* Note 2.

3 Methods

3.1 RNA Nanoparticle Preparation

1. DNA oligos were PCR amplified using the MyTaq™ Mix.
2. PCR products were purified using the DNA Clean and Concentrator™ kit.
3. Verification of PCR products was done using a 2% agarose gel stained with ethidium bromide. Samples were loaded and run for 10 min at 200 V, followed by visualization using a Bio-Rad ChemiDoc MP System.
4. RNAs for each of the six monomers were produced by in vitro run-off transcription using T7 RNA Polymerase in the buffer of the following composition: 80 mM HEPES-KOH, pH 7.5; 2.5 mM spermidine; 50 mM DTT; 25 mM MgCl2; 5 mM rNTPs.
5. RNAs were purified using an 8 M denaturing urea polyacrylamide gel electrophoresis (urea PAGE, 15%). RNA bands were visualized with a UV lamp (short wavelength), excised, and eluted overnight in "crush and soak" buffer.
6. RNAs were then precipitated by adding the "crush and soak" buffer to 2.5 volumes of 100% ethanol. The samples were then vortexed and placed in a − 20 °C freezer for 3 hours. Samples were spun down on a centrifuge at 14,000 rpm and rinsed with 90% ethanol twice, vacuum dried at a temperature of 55 °C, and then dissolved in ultra-pure water (17.8 MΩ·cm).
7. Concentration of each of the monomer strands was found by taking the absorbance of each strand using the NanoDrop.
8. To prepare the RNA nanoparticles (RNA rings), six RNA monomer strands were mixed at equimolar ratio in ddiH2O. The samples were heated to 95 °C for 2 min, snap-cooled to 4 °C for 2 min by placing the sample in an ice bucket, and assembly buffer was added before incubation at 30 °C for 30 min.

9. To verify the assembly of the RNA ring, an electrophoretic mobility shift assay was used. An 8% non-denaturing (native) PAGE (37.5:1) in the presence of 89 mM Tris-borate (pH 8.2), 2 mM $MgCl_2$.5 μL of1 μM RNA rings per well were loaded and the gel was run for 60 min at 4 °C, 300 V.
10. The gel was then stained with ethidium bromide for 5 min and then visualized using a Bio-Rad ChemiDoc MP System.

3.2 Mica Surface Modification with 1-(3-Aminopropyl)Silatrane (APS)

APS is not a commercially available reagent. It can be synthesized with standard equipment for organic chemistry as described in [5, 6].

1. Dissolve APS in ultrapure water to prepare a stock solution of 50 mM (*see* Note 3).
2. Immediately prior to surface modification, dilute stock solution 300 times with ultrapure water to the final concentration of C_{APS} = 167 μM (*see* Note 4).
3. Cut mica substrates into pieces of 1 × 3 cm^2 size using sharp scissors.
4. Cleave mica substrates using Scotch™ tape by peeling off layers on both sides of the substrate (*see* Note 5).
5. Place freshly cleaved mica substrates into a plastic cuvette filled with 167 μM APS solution, and leave for 30 min for modification.
6. Rinse mica substrates with ultrapure water a few times, and gently dry using ultra high purity argon.
7. Store APS-modified mica in vacuum overnight before sample deposition. Functionalized mica can be stored for several days under vacuum before use.

3.3 Deposition of RNA Nanoparticles on APS-Modified Mica Surface

Refer to Fig. 2 which illustrates the steps of sample preparation procedure outlined below.

1. Cut a small piece of APS-modified mica for sample deposition. Typical size necessary for AFM imaging is between 3 mm and 5 mm.
2. Place APS-modified piece of mica on a parafilm in a chamber designed to maintain constant humidity.
3. Deposit 2–5 μL of the sample solution in a dropwise manner (*see* Note 6).
4. Incubate for a total of 2 min.
5. Wash excess sample gently with copious amount of ultrapure water.
6. Gently dry the sample under a flow of ultra-high purity argon.
7. Store the deposited samples under vacuum overnight to remove residual water.

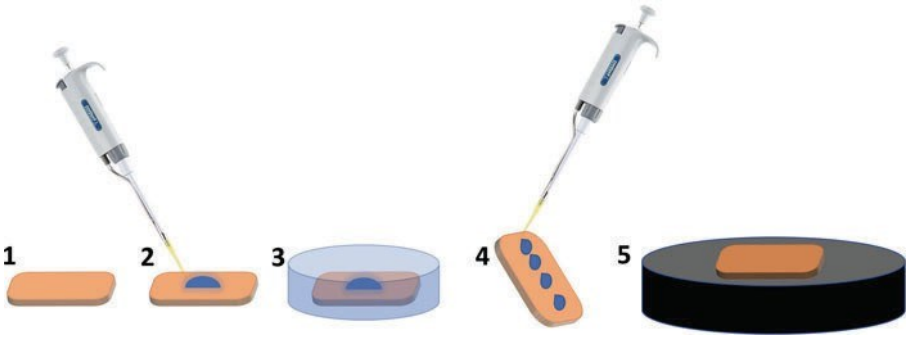

Fig. 2 Illustration of sample preparation procedure: (1) APS-modified mica, (2) deposit 2–5 μL of sample solution, (3) incubate for 2 min, (4) rinse with copious amount of ultrapure water, (5) mount on metal puck for imaging

3.4 Atomic Force Microscopy Imaging

3.4.1 Brief Overview

This chapter is not intended to describe in full the details of AFM imaging and its technical subtleties. For detailed description of AFM imaging procedure, we will refer readers to the following reviews [14, 15]. We focus on the practical aspects of imaging which might be of interest to non-specialists wishing to visualize nucleic acid-based nanostructures using AFM imaging in air. The imaging mode used in this protocol is TappingMode™—a Bruker-patented technique which allows for gentle imaging of nanostructures with an oscillating AFM probe. A high-resolution 3D image of the sample's surface topography is produced by monitoring the probe's amplitude/frequency of oscillation. It is crucial for high-resolution imaging to obtain a sample with clean background and optimal distribution of nanoparticles without crowding. It is important to note that chemical mica modification with APS provides stable fixation of nucleic acid-based nanostructures without their conformational distortion [14–17].

3.4.2 Atomic Force Microscopy Imaging

1. Place the AFM probe in the probe holder (*see* Note 8).
2. Mount the mica substrate with deposited sample onto a metal puck using double-sided adhesive tape.
3. Mount the metal puck onto the scanning stage of the AFM microscope. Scanning stages of Bruker's Nanoscope family of AFM are magnetic—designed to hold the metal pucks very well during imaging. The use of a scanner with small scan size is preferable, such as E-scanner from Bruker which is designed for up to 10 μm scan area.
4. Position and align the laser onto the AFM cantilever using laser adjustment knobs to maximize the sum.
5. Test if the laser is optimally reflected onto the quadrant detector by turning mirror's lever, and adjust to maximize the sum.

6. Adjust the horizontal deflection to a value as close to *0 V* as possible by using adjustment knobs.
7. Open imaging program and run the "Autotune" feature. *See* Note 9. Adjust the scan size to 100 × 100 nm^2, and start approaching the probe to the surface by pressing the "Engage" button. Scanning will start automatically once the probe is engaged. Change the scan size to 3 × 3 μm^2, the pixel size to 128, and the scan rate to 1.5 Hz. These settings will allow for fast surveying of the sample. Move to a different area if needed. Reduce the set point until the surface is being tracked well. Nanostructures will appear as bright spots on the image. Proceed to the next step when optimal number of complexes is found within the size of the image.
8. Zoom to a scan size below 1 μm to start high-resolution imaging.
9. Increase the number of pixels to 512, and decrease the scan rate to 1 Hz to acquire a topography image with high resolution. Adjust scanning parameters such as the drive amplitude, set point, and gains to values which produce desired high-quality appearance of nanostructures.
10. To avoid image distortions, several restarts on the scanning area are required before final image is scanned and saved as the scanner should be completely equilibrated on the selected area. Figure 3a shows a representative half of the image obtained for RNA nanorings, 0.6 × 0.3 μm^2, with 512 pixels.
11. If imaging of many nanostructures is required for statistical analysis, repeat steps 8–15 several times at different locations.

3.4.3 AFM Image Analysis to Evaluate Dynamicity of Nanoring Structures

AFM topography images can be processed using a variety of different software suites (*see* Note 1). We used the *FemtoScan Online* software package since it has a comprehensive set of tools for cross-sectional analysis and distance measurements, and it served very well for analysis of RNA nanostructures.

1. Open a file saved in Bruker imaging software. FemtoScan Online can read raw data file without any additional conversions.
2. Adjust the image scan line to the same mean level for the whole image—"leveling the image."
3. In the Z-scale settings, choose "brown" color palette and check "fixed scale" option.
4. Z-scale can be adjusted to achieve the desired visual contrast between RNA strands and background mica substrate.
5. For analysis of individual nanostructures, select rectangular area around a complex and choose "duplicate image" option. A separate window with the individual nanostructure of

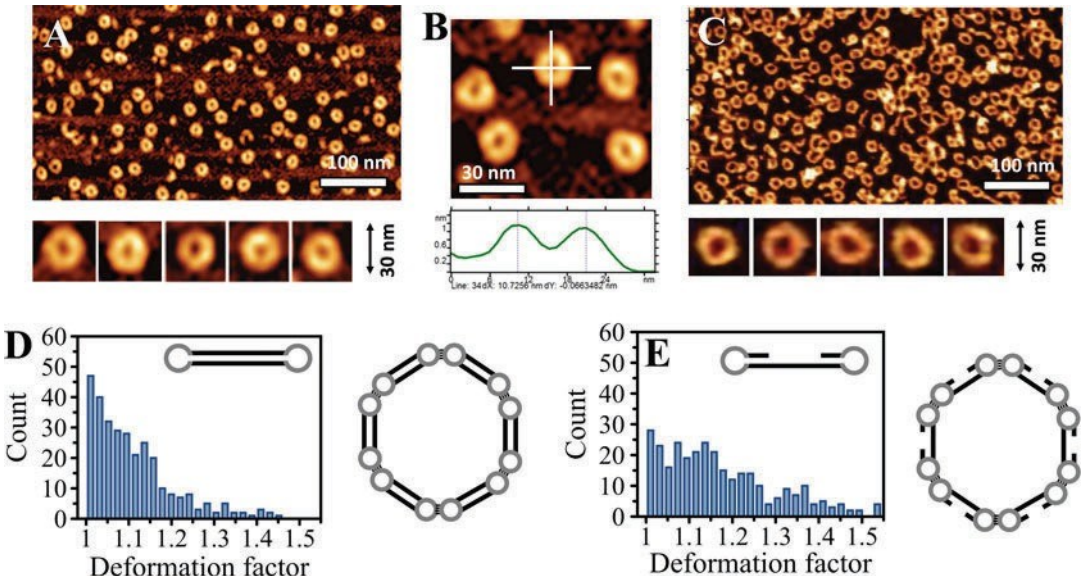

Fig. 3 (a) AFM topography image of RNA nanorings (600x300 nm^2), no gap construct. Bottom panel shows individual nanorings extracted from the images for deformation factor analysis. (b) Deformation factor (DF) is calculated as a ratio of distances between NA strands (maxima in the cross section through the center of NA ring) for perpendicularly placed vertical and horizontal cross-sectional lines. (c) AFM topography image of RNA nanorings (600x300 nm^2), 6 base gap construct. Bottom panel shows individual nanorings extracted from the images for deformation factor analysis. (d) Statistical histogram of DF values for "no gap" RNA nanoring. (e) Statistical histogram of D_F values for "6 base gap" RNA nanoring

interest will appear. Examples of 30 × 30 nm^2 areas with individual nanostructures are shown in Fig. 3a, c (bottom panels).

6. Using a "section" tool, build two orthogonal (long, L, along the major elliptical axis and short, SH, along the minor elliptical axis) cross-sectional lines (*see* Note 10). Each line will have a typical profile as shown in Fig. 3b.
7. Measure maximum-to-maximum distance in the cross-sectional profile for both major (D^L) and minor (D^{SH}) axes which report on the distance between segments of nucleic acids in the corresponding direction of the RNA ring assembly.
8. By taking the ratio of distances (D^L over D^{SH}), calculate the deformation factor (DF) (*see* Note 11).
9. Combine DF values in a statistical histogram using MagicPlot software (*see* Note 2). An example of such a statistical histogram is shown in Fig. 3d, e.
10. Compare DF values for structurally different RNA nanorings if needed (*see* Note 12).

4 Notes

1. Any other software with the capability of analyzing distance via cross-sectional line analysis could also be used including *WSxM*, *Gwyddion*, *ImageSXM*, and *ImageJ*.
2. Any other statistical software with the capability of plotting statistical histograms could also be used, for example, Excel (Microsoft, Inc.; Redmond, WA) or Origin Pro 2019 (OriginLab Corp., Northampton, MA).
3. There are several approaches utilized for the modification of mica substrate to obtain overall positively charged surface for effective binding of negatively charged RNA nanoparticles. One group of methods uses divalent cations such as Mg^{2+} and Ni^{2+} or other cations as a bridge between negatively charged surface groups and RNA nanoparticles. Another group of methods is based on chemical modification of the surface to create amino groups with reagents such as 3-aminopropyl-trietoxy silane (APTES) [14, 18–20] or 1-(3-aminopropyl)silatrane (APS) [5, 6]. Surface amino groups are positive at neutral pH providing strong enough binding for RNA. The modification procedure with APS is simple, is reproducible and provides a functionalized substrate for RNA or DNA sample deposition in a wide range of ionic conditions, temperatures, and pH values. APS allows to create positively charged surface for deposition of RNA, DNA, and DNA-protein complexes via electrostatic attraction between negatively charged nucleic acid backbone and positively charged APS-mica. This modification is very robust and reliable and has been extensively used in AFM studies. APS is an amorphous solid at normal conditions and is highly soluble in water. 1-(3-Aminopropyl)silatrane is not commercially available and requires custom synthesis [15, 16].
4. Use freshly diluted APS solution every time APS modification of mica is needed.
5. Typically, mica cleaving process is repeated several times until required quality of mica top layer is achieved. The quality of mica substrate is monitored by the appearance of the separated mica layer on the Scotch™ tape. The cleaving procedure of mica sheets is repeated until the surface of the cleaved mica layer on the Scotch™ tape is glossy and has no visible defects.
6. The concentration of RNA nanoparticles should be adjusted to provide optimal surface coverage where nanoparticles do not overlap on the AFM image. This can be achieved by making several depositions with stepwise dilutions (e.g., 1/10, 1/100, 1/1000) to optimize concentration of RNA nanoparticles.

7. Investigators who only begin using AFM imaging to visualize DNA and RNA nanostructures may encounter a few technical challenges. This chapter introduces specific details of AFM imaging and describes systematically the protocol and methods for obtaining good quality AFM topography images of RNA nanostructures. To obtain high-quality images, special attention should be paid to sample preparation procedures, the use of appropriate AFM probes, imaging mode, and imaging settings. These will contribute largely to the quality and reproducibility of AFM imaging. Also, we note that the AFM imaging approach described here is also broadly applicable to studying other nucleic acid nanostructures.
8. RTESPA-300 AFM probes were found to work reliably for imaging of DNA and RNA nanostructures in air. These probes have a nominal spring constant of 40 N/m and a resonance frequency at ~300 kHz. Although the nominal tip radius listed by the manufacturer is 8 nm, approximately one third of the probes are sharp enough to resolve subtle structural features of RNA nanostructures without any additional probe modifications.
9. The "autotune" feature in the imaging software will find the resonance peak of the cantilever and adjust the settings to the resonance frequency of the inserted AFM probe. Make sure that the target amplitude is at ~0.5 V and the drive amplitude is no larger than ~10 mV.
10. Using visual appearance of the nanostructures, determine the major (longest, L) and the minor (shortest, SH) axes of the elliptical nanostructures. Draw the lines such that they go through the center across the nanostructure. Make sure the lines maintain orthogonality.
11. Deformation factor is defined as $DF = D^{L}/D^{SH}$, where D^{L} is the longer distance along the major axis and D^{SH} is the shorter distance along minor axis of the elliptical nanostructure. The values of DF close to 1 will represent the least dynamic structure corresponding to a nearly circular shape of the nanostructure. Further improvement of the data analysis can be achieved via computer-assisted image analysis algorithm. This algorithm can identify circular objects on an AFM image and fit the nanostructures with an elliptical shape, automatically measuring major and minor axes of the ellipse. Such an approach allows for larger sets of structures to be analyzed [13].
12. DF is plotted as a statistical histogram for various designs of the RNA ring nano-assemblies. Stable rings will be mostly circular, while less stable structures adopt an apparent elliptical shape. DF, therefore, can be used as a measure of the susceptibility of the rings to deformation and their dynamic properties. Two

examples are shown in Fig. 3d, e to showcase the stark differences between stable RNA nanoring without any gaps and very flexible RNA nanoring which was modified with 6 base gaps in each monomeric dumbbell.

Acknowledgments

Research reported in this publication was supported by the National Science Foundation, Division of Material Research, Award Numbers 2203946 (to K.A.A.) and 2204027 (to A.V.K.), and by the National Institute of General Medical Sciences of the National Institutes of Health under Award Number R35GM139587 (to K.A.A.). The content is solely the responsibility of the authors and does not necessarily represent the official views of the National Institutes of Health. AFM imaging of the RNA nanostructures was performed at the nanoimaging core facility (University of Nebraska Medical Center).

References

1. Avila YI, Chandler M, Cedrone E, Newton HS, Richardson M, Xu J et al (2021) Induction of cytokines by nucleic acid nanoparticles (NANPs) depends on the type of delivery carrier. Molecules 26(3):625
2. Chandler M, Jain S, Halman J, Hong E, Dobrovolskaia MA, Zakharov AV et al (2022) Artificial immune cell, AI-cell, a new tool to predict interferon production by peripheral blood monocytes in response to nucleic acid nanoparticles. Small 18(46):e2204941
3. Chandler M, Johnson B, Khisamutdinov E, Dobrovolskaia MA, Sztuba-Solinska J, Salem AK et al (2021) The international society of RNA nanotechnology and nanomedicine (ISRNN): the present and future of the burgeoning field. ACS Nano 15(11): 16957–16973
4. Chandler M, Rolband L, Johnson MB, Shi D, Avila YI, Cedrone E et al (2022) Expanding structural space for immunomodulatory nucleic acid nanoparticles (Nanps) via spatial arrangement of their therapeutic moieties. Adv Funct Mater 32(43):43
5. Dobrovolskaia MA, Afonin KA (2020) Use of human peripheral blood mononuclear cells to define immunological properties of nucleic acid nanoparticles. Nat Protoc 15(11): 3678–3698
6. Rolband L, Beasock D, Wang Y, Shu YG, Dinman JD, Schlick T et al (2022) Biomotors, viral assembly, and RNA nanobiotechnology: current achievements and future directions. Comput Struct Biotechnol J 20:6120–6137
7. Tran AN, Chandler M, Halman J, Beasock D, Fessler A, McKeough RQ et al (2022) Anhydrous nucleic acid nanoparticles for storage and handling at broad range of temperatures. Small 18(13):13
8. Dey S, Fan C, Gothelf KV, Li J, Lin C, Liu L et al (2021) DNA origami. Nat Rev Method Primer 1(1):13
9. Afonin KA, Dobrovolskaia MA, Church G, Bathe M (2020) Opportunities, barriers, and a strategy for overcoming translational challenges to therapeutic nucleic acid nanotechnology. ACS Nano 14(8):9221–9227
10. Afonin KA, Dobrovolskaia MA, Ke W, Grodzinski P, Bathe M (2022) Critical review of nucleic acid nanotechnology to identify gaps and inform a strategy for accelerated clinical translation. Adv Drug Deliv Rev 181:114081
11. Yingling YG, Shapiro BA (2007) Computational design of an RNA hexagonal Nanoring and an RNA nanotube. Nano Lett 7(8): 2328–2334
12. Afonin KA, Viard M, Koyfman AY, Martins AN, Kasprzak WK, Panigaj M et al (2014) Multifunctional RNA nanoparticles. Nano Lett 14(10):5662–5671
13. Sajja S, Chandler M, Fedorov D, Kasprzak WK, Lushnikov A, Viard M et al (2018) Dynamic behavior of RNA nanoparticles analyzed by

AFM on a mica/air Interface. Langmuir 34(49):15099–15108

14. Lyubchenko YL, Gall AA, Shlyakhtenko LS (2014) Visualization of DNA and protein-DNA complexes with atomic force microscopy. Methods Mol Biol 1117:367–384
15. Lyubchenko YL, Shlyakhtenko LS, Gall AA (2009) Atomic force microscopy imaging and probing of DNA, proteins, and protein DNA complexes: silatrane surface chemistry. Methods Mol Biol 543:337–351
16. Shlyakhtenko LS, Gall AA, Lyubchenko YL (2013) Mica functionalization for imaging of DNA and protein-DNA complexes with atomic force microscopy. Methods Mol Biol 931:295–312
17. Lushnikov A, Hooy R, Sohn J, Krasnoslobodtsev A (2019) Characterization of DNA bound cyclic GMP-AMP synthase using atomic force microscopy imaging. Methods Enzymol 625: 157–166
18. Pie´trement O, Pastre´ D, Fusil S, Jeusset J, David M-O, Landousy F et al (2003) Reversible binding of DNA on NiCl2-treated mica by varying the ionic strength. Langmuir 19(7): 2536–2539
19. Bezanilla M, Manne S, Laney DE, Lyubchenko YL, Hansma HG (1995) Adsorption of DNA to mica, Silylated mica, and minerals: characterization by atomic force microscopy. Langmuir 11(2):655–659
20. Vesenka J, Guthold M, Tang CL, Keller D, Delaine E, Bustamante C (1992) Substrate preparation for reliable imaging of DNA molecules with the scanning force microscope. Ultramicroscopy 42-44(Pt B):1243–1249